*Journal of Mineralogical and Petrological Sciences, Volume 100, page 55–69, 2005*

# X-ray, DTA and Raman studies of monoclinic tridymite and its higher temperature orthorhombic modification with varying temperature

Tadayuki HIROSE[*], Kuniaki KIHARA[*], Masayuki OKUNO[*], Syuhei FUJINAMI[**] and Keiji SHINODA[***]

[*] *Department of Earth Sciences, Kanazawa University, Kakuma, Kanazawa 920–1192, Japan*
[**] *Department of Chemistry, Kanazawa University, Kakuma, Kanazawa 920–1192, Japan*
[***] *Department of Geosciences, Osaka City University, Sugimoto 3–3–138, Sumiyoshi, Osaka 558–8585, Japan*

Unit–cell parameters, Raman scattering profiles and DTA curves were measured on monoclinic tridymite from fired silica brick. Ten peaks appear in the Raman measurements from 100 to 1250 $cm^{-1}$ at 25 ℃, and their positions and widths show no significant change up to 110 ℃. The monoclinic unit–cell parameters, $a$, $b$, $c$ and $\beta$, slightly increase or remain nearly constant with increasing temperatures up to 110 ℃. Both the Raman spectra and the unit–cell parameters undergo significant changes in the range from 110 to 115 ℃. Only two endothermic peaks, at 117 and 166 ℃, appear in the DTA curve measured on a powdered sample of nearly pure monoclinic phase in a heating run from 25 to 300 ℃. In X–ray single–crystal refinements, the structural parameters including anisotropic temperature factors of atoms were fully determined for the monoclinic phase at 25, 80, 90 and 100 ℃, and the orthorhombic phase at 140 ℃. The difference between the temperature factors on both sides of the transition point is the most remarkable: 0.0286 $Å^2$ in average for all O atoms at 100 ℃ in the monoclinic phase and 0.0713 $Å^2$ at 140 ℃, both for $B_{eq}$. The averaged Si–O distances calculated for the atomic mean positions decrease with increasing temperatures: 1.599 Å at 25 ℃, 1.595 Å at 100 ℃ and 1.576 Å at 140 ℃, whereas the values corrected for the thermal displacement parameters remain unchanged at 1.61 Å through all the temperatures studied.

**Keywords**: Orthorhombic tridymite, Monoclinic tridymite, Phase transition, X–ray structure analyses, Temperature dependence, Raman spectra, DTA

## INTRODUCTION

Several meta–stable varieties of tridymite ($SiO_2$) have been reported under ambient conditions; the nomenclature of Nukui and Nakazawa (1978 and 1980) is used through this paper. These modifications can be divided into two main groups, monoclinic (MC) and pseudo–orthorhombic (PO). Most of the naturally occurring tridymites are PO with different unit–cells (Hoffman, 1967), whereas meteoritic (Dollase and Buerger, 1966) and synthetic ones (Hoffmann, 1967; Kato and Nukui, 1976) are MC. MC tridymite is also reported from fired silica bricks (Dollase and Buerger, 1966; Kihara, 1977; Schneider and Flölke, 1982) and from dacitic rocks in the Yugawara area, Japan, which is an exceptional case among the earths tridymites (Kawai et al., 1978).

K. Kihara, kuniaki@kenroku.kanazawa–u.ac.jp Corresponding author

With increasing temperatures, MC tridymite successively undergoes displacive structure transitions up to the hexagonal highest–temperature form (HP). The numbers of modifications observed in experiments show some variation, probably reflecting different conditions of crystallization or thermal history or so on. An X–ray single–crystal study (Nukui and Nakazawa, 1978) with heating experiments of synthetic MC tridymite showed a series of structure transitions such as MC–OP–OS–OC–HP, where OC, OS and OP are all orthorhombic. OC has a $C$–centered Bravais lattice, the primitive cell of which is only slightly distorted into orthorhombic from that of HP; and OP has the (3×1×1) superstructure cell of OC and OS with an incommensurate $a$–axis. OS also appears in the Steinbach meteorite (e.g., Dollase, 1967), but not in a MC crystal from fired silica brick (Kihara, 1978). Steinbach tridymite shows different transformation sequences for samples depending on whether they had been annealed or

not. OP appears only in the samples annealed in the stable field of HP (Cellai et al., 1994). In addition to these phases, according to Hoffmann et al., (1983), a phase MX–1 is obtained from mechanical or thermal treatment of MC crystals.

MX–1, which is incommensurately modulated with a monoclinic symmetry, was firstly reported by Nukui and Nakazawa (1980) for synthetic samples. Hoffmann et al. (1983) found that this phase is formed on heating MC crystals to temperatures ranging 110 to 160 ℃ and subsequent rapid cooling to −10 ℃, or by grinding or uniaxial compression of MC crystals, along the pseudohexagonal *c*–axis, at room temperature.

De Dombal and Carpenter (1993), in the DSC measurements of Steinbach tridymite, found two peaks at about 102 and 110 ℃ and also found, in their infrared (IR) measurements, a significant change of the wave number of a mode at about 800 $cm^{-1}$ at around 100 ℃. In the IR measurements of hand–ground Steinbach tridymite by Cellai et al. (1995), a band at 540 $cm^{-1}$ showed two discontinuities in the temperature dependence of the intensity at 75 and 100 ℃, and then disappeared at 115 ℃: these authors consider that the first discontinuity (at 75 ℃) is related to the (MX–1)–PO transition and the second one (at 100 ℃) to the MC–OS transition, which occurs at about 115 ℃. These data in the IR and DSC experiments lead Cellai et al. (1995) to conclude that the transition MC–OS or MC–OP apparently proceeds via an intermediate phase, which exists in a small temperature interval of about 12 ℃. The existence of the intermediate phase is also stressed by Pryde and Dove (1998) in a symmetry point of view for the related phases.

The crystal structure of MC has been studied so far only at room temperature. Dollase and Bauer (1976) and Kato and Nukui (1976) independently determined the structure at room temperature, employing different axial settings to each other. Both, however, led to the same space group symbol, *Cc*. In the present study, the *a*– and *c*–axes of Kato and Nukui (1976) are interchanged to make comparisons with the higher temperature modifications more convenient. The space group symbol is changed to *Aa* in this interchange. In MC (also in OP), multiple twinning commonly occurs in the six (three) orientations rotated around the pseudohexagonal *c*–axis, because this phase is, in general, obtained in cooling processes to the subgroups from the higher symmetry phases such as HP. The corresponding superstructure reflections from different orientations are separated from each other, and their intensity ratios may reflect the twin ratios. The specimens used in these previous studies were twinned, and intensities corrected for twinning were used in the refinement (Kato and Nukui, 1976; Dollase and Baur, 1976).

The OP structure has been refined in two studies so far, one with single crystal data (Kihara, 1977) and the other with Rietveld analysis of powder data (Graetsch, 2001). In Kihara (1977), 428 intensities below $\sin\theta/\lambda = 0.46$ $Å^{-1}$ were used to determine the 163 parameters in an anisotropic temperature–factor model. Because of the scarcity of observed reflections, it was not possible simultaneously to determine the full set of variable parameters in the anisotropic model.

The present study was undertaken with three main purposes: the first is to determine the crystal structures of MC and OP at various temperatures above room temperature, the second to establish the structural relationship between MC and OP, and the third to measure spectroscopic data of monoclinic tridymite with varying temperatures. For the first, X–ray single–crystal intensities were newly measured with a nearly twin–free crystal on a diffractometer equipped with a charge–coupled device (CCD) detector. For the second, DTA measurements were carried out on powdered samples prepared to be of the single phase of MC tridymite, and the unit–cell parameters were measured with a single–crystal at various temperatures including the MC–OP transition point, focusing on the reported intermediate phase (Cellai et al., 1995). For the third, Raman spectroscopic data were measured for MC, OP and the higher temperature phases of tridymite: these data are not only the first to be reported but are informative in respect of the second objective. In addition to these main objectives, X–ray powder diffraction measurements were carried out to examine the effects of grinding or heat treatment during preparation of samples of MC.

## EXPERIMENTAL

### Sample preparation

Transparent crystalline specimens grown on the surface of refractory silica brick, which had enjoyed much the same thermal history as that used in our previous papers (e.g., Kihara, 1977), were scratched from the surface and used to prepare specimens for the X–ray, DTA and Raman measurements.

In the present measurements, both powdered samples and single–crystals (or fragmental crystals) were used. The powdered samples were prepared by three different procedures. The aggregate of crystals collected from the scratch were hand–ground in a mortar to prepare the first sample, which is hereafter called TP–r. A part of the TP–r powders was repeatedly treated, more than ten times, by heating up to 250 ℃ in air and by subsequent

**Table 1.** Unit–cell parameters of monoclinic tridymite, MC, in space group *Aa* with varying temperature, determined with a single–crystal specimen

| Temperature(°C) | *a*(Å) | *b*(Å) | *c*(Å) | *β*(°) |
|---|---|---|---|---|
| 25 | 25.878(3) | 5.001(8) | 18.526(2) | 117.69(1) |
| 50 | 25.891(2) | 5.002(6) | 18.526(2) | 117.71(1) |
| 60 | 25.904(2) | 5.005(6) | 18.530(2) | 117.74(1) |
| 70 | 25.900(4) | 4.000(2) | 18.534(3) | 117.72(1) |
| 80 | 25.906(4) | 5.001(2) | 18.539(3) | 117.73(1) |
| 85 | 25.916(2) | 5.003(6) | 18.540(2) | 117.74(1) |
| 90 | 25.917(3) | 5.003(8) | 18.539(2) | 117.73(1) |
| 95 | 25.916(4) | 5.001(2) | 18.544(3) | 117.72(1) |
| 100 | 25.919(4) | 5.004(2) | 18.540(3) | 117.72(1) |
| 103 | 25.931(3) | 5.005(8) | 18.544(2) | 117.75(1) |
| 106 | 25.928(3) | 5.005(8) | 18.548(2) | 117.72(1) |
| 110 | 25.925(2) | 5.008(7) | 18.545(2) | 117.74(1) |
| 115* | 26.165(2) | 4.982(5) | 18.570(2) | 118.02(1) |
| 120* | 26.162(4) | 4.983(5) | 18.572(2) | 118.03(1) |
| 125* | 26.164(5) | 4.982(7) | 18.572(3) | 118.02(1) |

ESDs are in parentheses.
* Above 115 ℃, the structure is orthorhombic, but values shown are calculated for reflections indexed as the monoclinic cell.

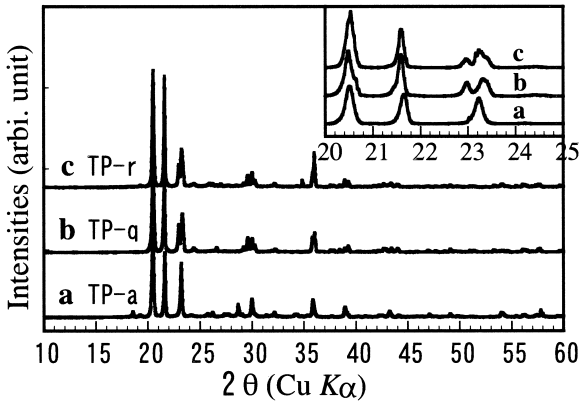


**Figure 1.** X–ray powder diffraction diagrams (Cu $K\alpha$) of tridymite prepared by different treatments. **a** TP–a, **b** TP–q and **c** TP–r. Details from $2\theta$=20 to 25 °are shown in the inlet.

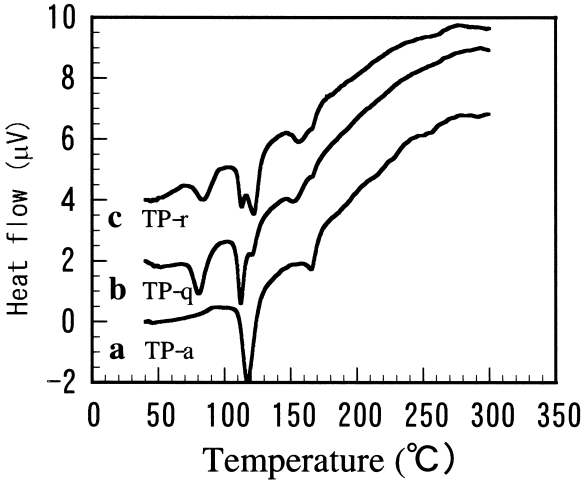


**Figure 3.** DTA curves in heating runs with a heating rate of 7 ℃/min. **a** TP–a, **b** TP–q and **c** TP–r.

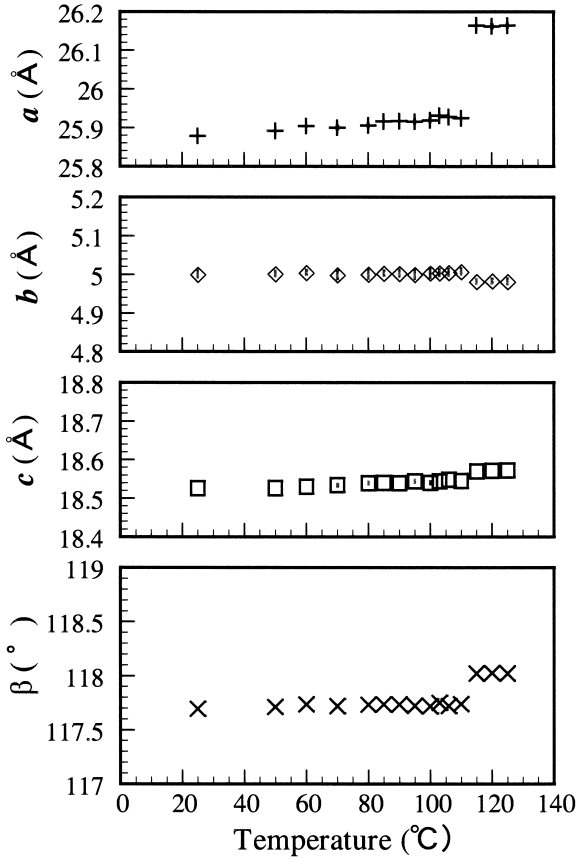


**Figure 2.** Temperature dependence of monoclinic unit–cell dimensions, *a*, *b* and *c* (Å), and angles $\beta$ ( °) from 25 to 110 ℃, measured with a single–crystal on a 4–circle diffractometer. Corresponding values for the orthorhombic phase, calculated for the reflections indexed with the monoclinic cell, are also indicated for three temperatures from 115 to 125 ℃.

cooling down to −30 ℃ in ethanol. This is called TP–q. The third sample was prepared by the continuous heating of a mixture of the TP–r powders and reagent grade $Na_2WO_4.2H_2O$ powder over 96 hrs at 900 ℃. After cooling, the mixture was washed by repeated watering at 50 ℃ to remove the tungstate powder. The residual powder ample was called TP–a. According to Graetsch (2001), powdered samples of MC are obtained from MX–1 in this treatment.

Experiments on single–crystals or fragmental specimens are very important for the studies of the structural changes in tridymite to avoid external stresses on the samples during sample preparations. The Raman spectra and X–ray integrated intensities were measured on two groups of fragments of different sizes, one 0.2–0.3 mm and the other smaller than 0.1 mm in three dimensions. The specimens with dimensions 0.2–0.3 mm are almost always twinned, convenient for the Raman measurements. In contrast, on examining diffraction patterns using a single crystal diffractometer with a CCD detector, we found some of the smaller–sized fragments to be nearly free from twinning.

**X-ray powder diffractions and single-crystal measurements of unit-cells**

Figure 1 shows the powder diffraction diagrams of the three kinds of samples, **a** for TP–a, **b** for TP–q and **c** for TP–r, all measured at room temperature with a diffractometer RINT2000 (Rigaku Co.). All the observed peaks for TP–a were indexed with the monoclinic cell in the *Aa* setting, and its constants were determined with least–squares fitting as $a$=25.45(7), $b$=4.93(1), $c$=18.24(5)Å and $\beta$=117.0(2) °. We conclude at this stage that TP–a is MC. However, the diffraction patterns for TP–r and TP–q appear slightly different from TP–a, having three or two peaks around $2\theta$ of 23 °(the inlet of Fig. 1). After consulting Graetsch (1998), we conclude that TP–q is MX–1, whereas TP–r is a mixture of MX–1 and MC.

The temperature dependences of the unit–cell dimensions in the range from room temperature to 125 ℃ were measured on a twin–free fragment of MC using a 4–circle diffractometer. The specimen was heated with an electric furnace mounted on the diffractometer, and the temperatures at the specimen were calibrated with the melting points of Sn, Zn and Pb. The accuracies were estimated to be better than 1 ℃ in the range of the present measurements (details are given in Kihara, 1990). The values of the unit–cell dimensions determined in least squares fitting are tabulated in Table 1 and plotted in Figure 2. The $a$– and $c$–dimensions increase only slightly with increasing temperature in MC, the $b$–dimension stays nearly constant, and there is just one abrupt change occurring between 110 and 115 ℃ for each dimension.

**DTA measurement**

DTA curves were measured on the three kinds of powdered samples with a TG8120 (Rigaku Co.): the results for the heating measurements are shown in Figure 3. The heating rate was 7 ℃/min and $Al_2O_3$ was used as the standard. Below 300 ℃, TP–r shows at least five endothermic peaks at about 84, 113, 122, 155 and 168 ℃, all read at the top position. The five peaks are also observed in TP–q, but the peak positions and heights are obviously changed to 80, 112, 121, 152 and 166 ℃, respectively. On the contrary, TP–a shows a simple DTA pattern with only two endothermic peaks at about 117 ℃ and 166 ℃: the former is possibly related to the MC–OP transition and the latter to the OP–OC transition or OP–OS transition. In comparison with the results of Graetsch (1998), the present DTA curve of TP–a appears almost equal with that of MC, whereas that of TP–q, which we consider as MX–1 by comparison of the X–ray diffraction patterns, appears different from Graetschs MX–1, which lacks the peak at 121 ℃, but has an additional peak at about 200 ℃.

**Raman measurement**

The Raman spectra at 29 temperatures from 25 to 500 ℃ were measured on a fragmental crystal of MC (dimension of about 0.25 mm) in an argon laser beam of diameter 100 $\mu$m, using a Raman microscope spectrometer, STR250 (Seki Technotron Co.). The powdered sample TP–q was also measured at 19 temperatures. Figure 4 shows the spectra for the selected temperatures measured on the fragmental crystal (**a**) and the powdered sample TP–q (**b**). The Raman spectra of the powdered sample TP–q have broad peaks at about 225, 295, 360, 445, 790 and 1080 $cm^{-1}$ and compare well with those observed above 115 ℃ for the fragmental specimen. It is reasonable to assume that, under the present experimental conditions, all the possible phonon modes, or at least those given by a powdered sample, are available with the fragmental crystal.

Both the MC and OP structures have 72 atoms in their primitive cells. The 213 species of optic modes at the zone center $\Gamma$ are all Raman active for both MC and OP. For the measured spectra of MC, we see only ten peaks below 1250 $cm^{-1}$: several peaks are concentrated into a range from 200 to 500 $cm^{-1}$, and others are in ranges 750–800 $cm^{-1}$ and 1000–1250 $cm^{-1}$, indicating that narrowly separated bands contribute to each of the individual peaks. We assign sequential numbers to the peaks

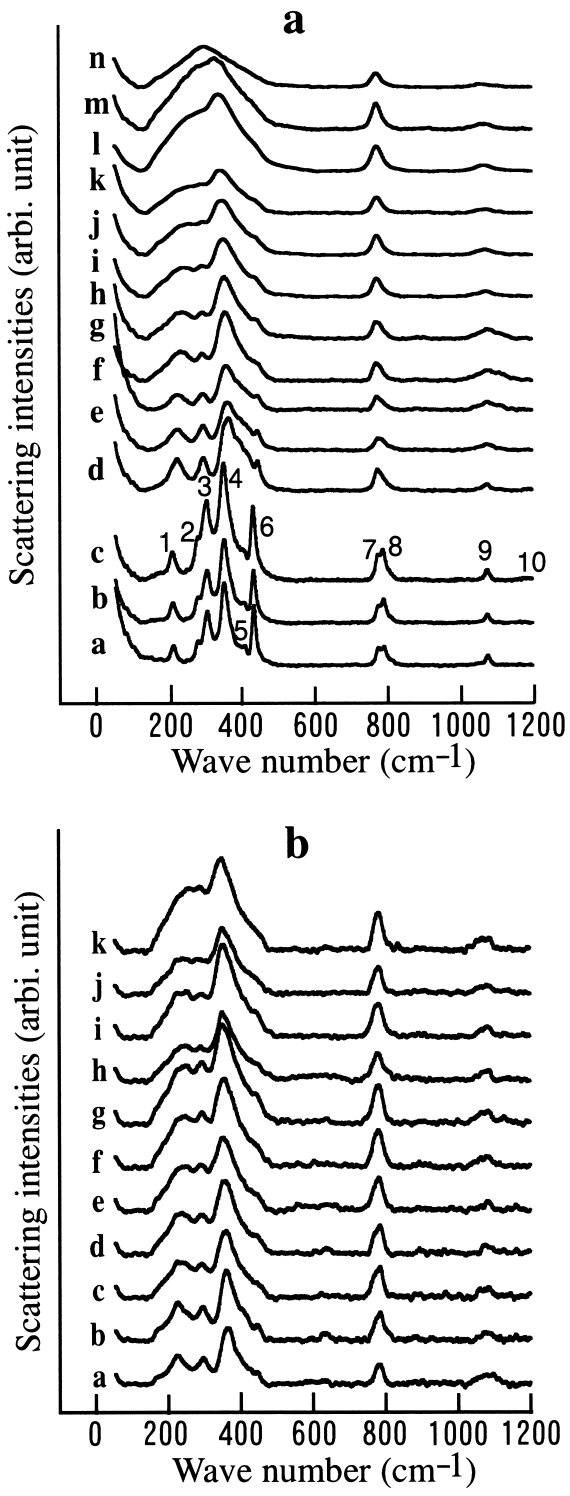


**Figure 4.** Raman spectra at varying temperatures: **a** for 14 selected points of temperature for a fragmental specimen, and **b** for 11 selected points of temperature for powdered specimen TP–q. Temperatures for a are **a**; 25, b; 70, c; 110, d; 115, e; 140, f; 160, g; 180, h; 200, i; 240, j; 280, k; 300, l; 360, m; 420 and n; 500 ℃, and for **b** a; 40, b; 50, c; 80, d; 90, e; 100, f; 110, g; 120, h; 130, i; 140, j; 150 and k; 210 ℃. An argon laser beam of diameter 100 $\mu$m was used. The resolution in wave number is 1.3 $cm^{-1}$, and intensities were accumulated over 30 single measurements for 10 s.

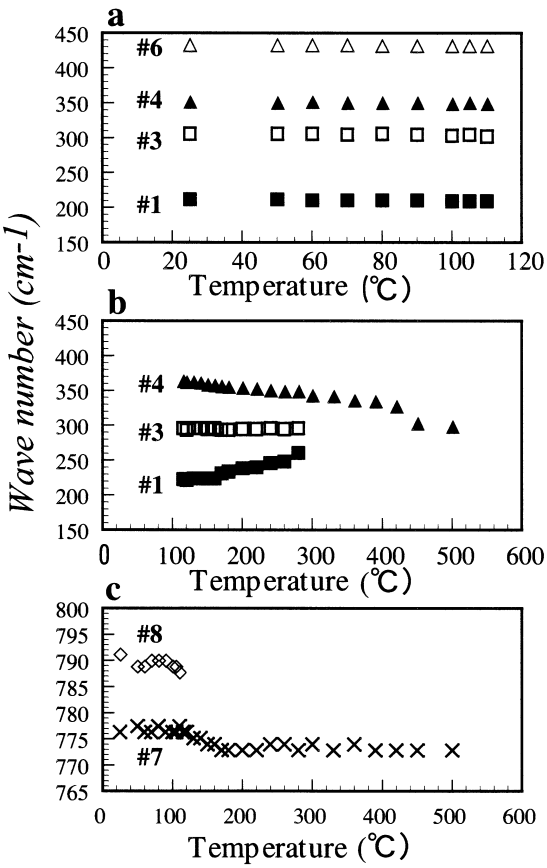


**Figure 5.** Temperature dependences of wave numbers of selected Raman peaks.
**a** Peaks #1, #3, #4 and #6 in MC from 25 to 110 ℃ are represented with ■ , □ , ▲ and △ , respectively; **b** Peaks #1, #3 and #4 for temperatures above 110 to 500 ℃ (c) peaks #7 and #8 with and ◇ , respectively, from 25 to 500 ℃.

(Fig. 4a), whose positions are represented by the wave numbers read from the top of the peaks. Because the peaks are contributed by some numbers of modes, the wave numbers assigned are only for the convenience of explanation and do not correspond to any real phonon mode. The measured peaks for the higher temperature forms are apparently broader than those for MC, but the basic features remain almost unchanged, with only slight peak shifts and intensity changes.

Figure 5 exhibits the temperature dependences of such *wave numbers* of selected peaks up to 500 ℃: the top positions are read after smoothing. The peaks observed at room temperature are relatively sharp and show no significant changes in their positions and widths up to 110 ℃ (Figs. 4a and 5a). The Raman profiles at 110 and 115 ℃ are obviously different (Fig. 4a), showing that a structural transition occurs between these temperatures. The change apparently corresponds to the peak at 117 ℃ in the DTA curve, considered as the MC–OP transition.

Above 115 ℃, peak #2 disappears or is unified to a single broad peak at the #3 position (Fig. 4a). Peaks #7 and #8 are separated in MC, but the latter appears to weaken to a shoulder of the former in the higher temperature phase (Fig. 4a). The *wave numbers* of peaks #1 and #7 show gaps at about 170 ℃ (Fig. 5b, c), which corresponds to the peak in DTA, considered as the OP–OC transition. The *wave numbers* of peaks #1 and #4 in OP and OC show weak but steady temperature dependence with increasing temperature, the former moves toward the higher wave number side, but the latter moves to lower wave numbers. The three peaks, #1, #3 and #4, at about 220, 300 and 360 $cm^{-1}$ at 110 ℃, become a single broad peak at about 300 $cm^{-1}$ between 420 and 450 ℃. These values of temperatures remind us of the OC–HP transition point at about 420 ℃, which was observed in the previous X–ray single–crystal study (Kihara, 1978).

## STRUCTURE-REFINEMENT

The integrated intensities were measured with a graphite monochromatized Mo $K\alpha$ radiation on the CCD diffractometer at 25, 80, 90, 100 and 140 ℃ using a fragment, of size $0.1\times0.1\times0.05$ $mm^3$, which showed no obvious sign of twinning. The crystal was bathed in a heated airflow, the temperature of which was monitored and controlled within $\pm$ 1 ℃. The space groups were confirmed by examining the intensity distributions and systematic absences: at the four points of temperatures, 25, 80, 90 and 100 ℃, it is monoclinic *Aa* with the unit–cell used in

**Table 2.** Conditions of intensity measurements, structure refinements and crystallographic data

| | Monoclinic tridymite MC (space group *Aa*, Z = 12) | | | | Orthorhombic tridymite OP (space group $P2_12_12_1$, Z = 6 ) |
|---|---|---|---|---|---|
| Temperature (°C) | 25 | 80 | 90 | 100 | 140 |
| Radiation | Mo $K\alpha$, $2\theta_{max.}$: 60° | | | | |
| Image width | 0.5° | | | | |
| Exposure time | 20 s for all measurements | | | | |
| Number of reflections | | | | | |
| measured | 10113 | 10104 | 10138 | 10175 | 8290 |
| independent $\|F_o\|>0$ | 2696 | 2695 | 2707 | 2711 | 1620 |
| independent $\|F_o\|>\sigma$ | 2251 | 2239 | 2229 | 2226 | |
| independent $\|F_o\|>3\sigma$ | 1655 | 1625 | 1592 | 1598 | 336 |
| Unit-cell parameters | | | | | |
| a (Å) | 25.878(3) | 25.906(4) | 25.917(3) | 25.919(4) | 26.163(9) |
| b (Å) | 5.001(8) | 5.001(2) | 5.003(8) | 5.004(2) | 4.987(2) |
| c (Å) | 18.526(2) | 18.539(3) | 18.539(2) | 18.540(3) | 8.199(3) |
| β (°) | 117.69(1) | 117.73(1) | 117.73(1) | 117.72(1) | ----- |
| Number of parameters | 325[*1] (1 scale + 108 coordinates + 216 anisotropic temperature factor coefficients) | | | | 163 (1 scale + 54 coordinates + 108 anisotropic temperature factor coefficients) |
| $R$[*2] | | | | | |
| $\|F_o\|>0$ | | | | | 0.131 |
| $\|F_o\|>\sigma$ | 0.059 | 0.063 | 0.064 | 0.065 | |
| $\|F_o\|>3\sigma$ | 0.039 | 0.041 | 0.041 | 0.042 | 0.041 |
| $R_w$[*3] | | | | | |
| $\|F_o\|>0$ | | | | | 0.089 |
| $\|F_o\|>\sigma$ | 0.040 | 0.044 | 0.042 | 0.039 | |
| $\|F_o\|>3\sigma$ | 0.036 | 0.040 | 0.037 | 0.035 | 0.051 |
| GOF (Goodness-of-fit) | | | | | |
| $\|F_o\|>0$ | | | | | 0.78 |
| $\|F_o\|>\sigma$ | 1.40 | 1.42 | 1.39 | 1.44 | |
| $\|F_o\|>3\sigma$ | 1.40 | 1.38 | 1.36 | 1.41 | 0.91 |

[*1] Two coordinates *x* and *z* for $Si_1$ were fixed during the refinements to define the origin.

[*2] $R = \Sigma||F_o| - |F_c|| / \Sigma|F_o|$

[*3] $R_w = \{\Sigma[w(|F_o| - |F_c|)^2] / \Sigma wF_o^2\}^{1/2}$

the indexing of the present powder diffraction diagram and, at 140 ℃, orthorhombic $P2_12_12_1$ with the unit–cell of OP. These data are summarized in Table 2. The integrated intensity for each reflection was processed with TEXSAN™ (1989) to prepare and estimate its structure factor amplitude $|F_o|$ and standard deviation $\sigma(|F_o|)$, respectively. The symmetrically independent $|F_o|$ values were obtained by averaging over the equivalent ones. Most of the superstructure reflections, particularly in OP, are of weak intensity: the number of observed reflections in an asymmetric unit was 1620 for OP (in the measurement at 140 ℃) and about 2700 for MC (in the four measurements). Among those, 336 and about 1600 reflections were of $|F_o|$ values larger than or equal to the corresponding $3\sigma$ for OP and MC, respectively. To improve the ratios of parameters to observations, all the measured reflections were used in the refinements for OP whereas, for MC, the number of the reflections with $|F_o|$ greater than or equal to one $\sigma$ was sufficient to achieve a reasonable condition for the least squares refinement. The least–squares program LSGCEX (Kihara, 1990) was used.

The refinement was commenced with the OP structure at 140 ℃. The initial atomic coordinates were obtained from the OC structure by applying a program KEY (Ito, 1973). The refinement initiated with these coordinates resulted in the $R_w$ value of 0.089 for 1620 reflections with the 163 variable parameters: a scale factor and 162 atomic parameters for the 18 symmetrically independent atoms on the general potions of $P2_12_12_1$ (Table 2). It is noted that, if the structure factors are calculated only for the reflections with $|F_o|$ values larger than or equal to corresponding 3 $\sigma$ s, the agreement factor $R_w$ reduces to 0.051 for 336 reflections. The present atomic coordinates are essentially the same as those of Kihara (1977) in their displacement directions from the OC structure, whereas some differences are seen in the coordinates and temperature factors in the view of the estimated standard deviations (ESDs). The present values are considered to be more accurate because they take account of the remarkable increase in observations, enabling us to refine all the variable parameters simultaneously. The intensity data for OP were measured only at 140 ℃, and the atomic parameters, atomic distances and angles are listed in Table 3.

The series of refinements at the four temperatures in the field of MC was initiated with the 100 ℃ data, employing the atomic coordinates determined in applying program KEY to the OP parameters at 140 ℃ determined as above. The refinements were carried out varying 323 parameters simultaneously: a scale factor and 322 atomic parameters for the 36 symmetrically independent atoms on the general potions of *Aa*. During the refinements, the two coordinates, *x* and *z*, for $Si_1$ were fixed to define the origin. The parameters obtained for the 100 ℃ data were

**Table 3.** The atomic parameters, distances and angles in orthorhombic tridymite, OP, at 140 ℃

(a) Positional parameters and equivalent isotropic temperature factors, $B_{eq}$

| Atom* | *x* | *y* | *z* | $B_{eq}$ (Å$^2$) |
|---|---|---|---|---|
| $Si_1$ | 0.1390(1) | 0.6112(7) | 0.6786(5) | 2.23(6) |
| $Si_2$ | 0.1393(1) | 0.4957(7) | 0.3012(5) | 2.56(6) |
| $Si_3$ | 0.0278(1) | 0.6180(7) | 0.8118(5) | 2.53(6) |
| $Si_4$ | 0.0282(1) | 0.5019(7) | 0.1843(4) | 2.06(6) |
| $Si_5$ | 0.1946(1) | 0.1131(7) | 0.8013(5) | 2.42(6) |
| $Si_6$ | 0.1945(1) | 0.9954(8) | 0.1740(6) | 3.03(7) |
| $O_1$ | 0.1935(5) | 0.058(3) | 0.986(2) | 7.6(4) |
| $O_2$ | 0.1403(6) | 0.565(3) | 0.490(2) | 7.6(4) |
| $O_3$ | 0.0299(6) | 0.568(3) | 0.001(2) | 7.2(3) |
| $O_4$ | 0.0825(3) | 0.563(2) | 0.743(2) | 6.0(3) |
| $O_5$ | 0.0823(3) | 0.428(2) | 0.241(2) | 5.9(3) |
| $O_6$ | 0.2484(3) | 0.914(2) | 0.234(2) | 5.4(3) |
| $O_7$ | 0.1762(3) | 0.412(2) | 0.765(2) | 3.8(2) |
| $O_8$ | 0.1754(3) | 0.253(2) | 0.275(2) | 5.2(3) |
| $O_9$ | 0.1564(3) | 0.910(2) | 0.715(2) | 4.5(3) |
| $O_{10}$ | 0.1572(4) | 0.754(3) | 0.199(2) | 5.7(3) |
| $O_{11}$ | -0.0107(3) | 0.418(2) | 0.727(2) | 4.3(2) |
| $O_{12}$ | -0.0089(3) | 0.251(2) | 0.215(2) | 4.4(3) |

ESDs are in parentheses.

* Atoms are all on general positions of space group $P2_12_12_1$.

The origin is placed as in the standard setting.

**Table 3.** (Continued.)
(b) Si–O distances (Å), Si–Oi – Si( °) angles and O–O distances (Å)

Si-O distances (Å)

| Si-O | Uncor-rected | Cor-rected | Si-O | Uncor-rected | Cor-rected | Si-O | Uncor-rected | Cor-rected |
|---|---|---|---|---|---|---|---|---|
| $Si_1$ - $O_2$ | 1.560(10) | 1.62(3) | $Si_2$ - $O_2$ | 1.590 (10) | 1.65(3) | $Si_3$ - $O_3$ | 1.570(10) | 1.63(3) |
| $Si_1$ - $O_4$ | 1.588(8) | 1.63(2) | $Si_2$ - $O_5$ | 1.608(7) | 1.65(2) | $Si_3$ - $O_4$ | 1.563(8) | 1.60(3) |
| $Si_1$ - $O_7$ | 1.560(8) | 1.58(2) | $Si_2$ - $O_8$ | 1.549(8) | 1.58(2) | $Si_3$ - $O_{11}$ | 1.581(8) | 1.60(3) |
| $Si_1$ - $O_9$ | 1.585(9) | 1.61(2) | $Si_2$- $O_{10}$ | 1.610(10) | 1.65(2) | $Si_3$ - $O_{11}$ | 1.592(8) | 1.61(3) |
| Mean | 1.573 | 1.61 | Mean | 1.589 | 1.63 | Mean | 1.577 | 1.61 |
| $Si_4$ -$O_3$ | 1.540(10) | 1.60(3) | $Si_5$ -$O_1$ | 1.540(1) | $1.60_3$ | $Si_6$ - $O_1$ | 1.570(10) | 1.62(3) |
| $Si_4$- $O_5$ | 1.536(7) | 1.58(2) | $Si_5$ -$O_6$ | 1.597(8) | $1.63_2$ | $Si_6$ - $O_6$ | 1.548(8) | 1.58(2) |
| $Si_4$- $O_{12}$ | 1.603(8) | 1.63(2) | $Si_5$ -$O_7$ | 1.594(7) | $1.61_2$ | $Si_6$ - $O_8$ | 1.610(10) | 1.64(2) |
| $Si_4$- $O_{12}$ | 1.574(9) | 1.60(2) | $Si_5$ -$O_9$ | 1.591(9) | $1.62_2$ | $Si_6$ - $O_{10}$ | 1.560(10) | 1.59(2) |
| Mean | 1.563 | 1.60 | Mean | 1.581 | 1.62 | Mean | 1.572 | 1.61 |

Mean Si-O (uncorrected, corrected)* : 1.576, 1.61

Si-O-Si angles (°)

| Si-O-Si | Uncor-rected | Cor-rected | Si-O-Si | Uncor-rected | Cor-rected | Si-O-Si | Uncor-rected | Cor-rected |
|---|---|---|---|---|---|---|---|---|
| $Si_5$-$O_1$-$Si_6$ | 177.7(9) | 149(3) | $Si_1$-$O_2$-$Si_2$ | 175.0(10) | 148(2) | $Si_1$-$O_3$-$Si_4$ | 175.0(10) | 149(2) |
| $Si_1$-$O_4$-$Si_3$ | 161.0(7) | 148(2) | $Si_2$-$O_5$-$Si_4$ | 153.8(6) | 143(1) | $Si_5$-$O_6$-$Si_6$ | 169.5(8) | 155(2) |
| $Si_1$-$O_7$-$Si_5$ | 150.3(6) | 148(2) | $Si_2$-$O_8$-$Si_6$ | 152.4(8) | 145(2) | $Si_1$-$O_9$-$Si_5$ | 149.6(7) | 142(1) |
| $Si_2$-$O_{10}$-$Si_6$ | 150.1(7) | 142(2) | $Si_3$-$O_{11}$-$Si_3$ | 149.3(5) | 144(2) | $Si_4$-$O_{12}$-$Si_4$ | 153.3(6) | 146(2) |

Mean Si-O-Si(∥) (uncorrected, corrected)* : 154.4, 146
Mean Si-O-Si(⊥) (uncorrected, corrected)*: 175.9, 149
Mean Si-O-Si(uncorrected, corrected)* : 159.8, 147

O-O distances (uncorrected) (Å)

| $Si_1$ | $Si_2$ | $Si_3$ |
|---|---|---|
| $O_2$-$O_4$: 2.57(2), $O_2$-$O_7$: 2.56(2) | $O_2$-$O_5$: 2.64(2), $O_2$-$O_8$: 2.53(2) | $O_3$-$O_4$: 2.52(2), $O_3$-$O_{11}$: 2.59(1) |
| $O_2$-$O_9$: 2.55(2), $O_4$-$O_7$: 2.57(1) | $O_2$-$O_{10}$: 2.61(2), $O_5$-$O_8$: 2.60(1) | $O_3$-$O_{11}$: 2.60(1), $O_4$-$O_{11}$: 2.55(1) |
| $O_4$-$O_9$: 2.60(1), $O_7$-$O_9$: 2.57(1) | $O_5$-$O_{10}$: 2.57(1), $O_8$-$O_{10}$: 2.61(2) | $O_4$-$O_{11}$: 2.59(1), $O_{11}$-$O_{11}$: 2.58(1) |
| $Si_4$ | $Si_5$ | $Si_6$ |
| $O_3$-$O_5$: 2.50(2), $O_3$-$O_{12}$: 2.57(1) | $O_1$-$O_6$: 2.59(2), $O_1$-$O_7$: 2.57(2) | $O_1$-$O_6$: 2.57(2), $O_1$-$O_8$: 2.60(2) |
| $O_3$-$O_{12}$: 2.56(1), $O_5$-$O_{12}$: 2.55(1) | $O_1$-$O_9$: 2.54(2), $O_6$-$O_7$: 2.57(1) | $O_1$-$O_{10}$: 2.50(2), $O_6$-$O_8$: 2.57(1) |
| $O_5$-$O_{12}$: 2.53(1), $O_{12}$-$O_{12}$: 2.60(1) | $O_6$-$O_9$: 2.65(1), $O_7$-$O_9$: 2.59(1) | $O_6$-$O_{10}$: 2.53(1), $O_8$-$O_{10}$: 2.62(2) |

Mean O-O *: 2.57

Si–O distances and Si–O–Si angles are shown as“ uncorrected ”for those calculated with mean positions of related atoms, and as“ corrected ”for those corrected for thermal displacement factors of related atoms. O–O distances are only for uncorrected. ESDs are in parentheses.
* Unbiased estimates of sample means.

used as the starting values of the subsequent refinements for the next lower temperature data to room temperature. The $R_w$ –factors, about 0.04 for about 2250 reflections with $|F_o|$ values larger than or equal to the corresponding $\sigma$ s and about 0.035 for about 1600 $|F_o|$ values larger than or equal to the corresponding 3 σ, are improved in comparison with the literature values. In Table 4, (a) the atomic coordinates and equivalent isotropic temperature factors, (b) the Si–O distances, (c) the Si–O–Si angles and (d) the O–O distances are listed for the cases of 25 and 100 ℃. The full structural parameters and the sets of $|F_o|$ are not presented here, but may be available from the authors on request.

## STRUCTURAL DESCRIPTION

Figure 6a shows the projections of the OP structure at 140 ℃ on (001) and (010), and Figure 6b the projection of the MC structure at 100 ℃ on (010), where atoms are represented by the thermal ellipsoids of 50 % probabilities.

**Table 4.** Atomic parameters (a), Si–O distances (b), Si–O–Si angles (c) and O–O distances (d) in monoclinic tridymite, MC, at 25 and 100 ℃

(a) Atomic coordinates and equivalent isotropic temperature factors

| Atoms[*1] | *x* | | *y* | | *z* | | $B_{eq}$ (Å$^2$) | |
|---|---|---|---|---|---|---|---|---|
| | 25 °C | 100 °C | 25 °C | 100 °C | 25 °C | 100 °C | 25 °C | 100 °C |
| $Si_1$ | -0.0179[*2] | -0.0179[*2] | 0.6982(6) | 0.7013(6) | 0.0314[*2] | 0.0314[*2] | 0.89(4) | 1.18(4) |
| $Si_2$ | 0.0108(1) | 0.0112(1) | 0.1979(6) | 0.2006(6) | -0.0393(1) | -0.0383(1) | 0.90(4) | 1.11(4) |
| $Si_3$ | 0.1468(1) | 0.1469(2) | 0.2112(5) | 0.2121(6) | 0.0469(2) | 0.0459(2) | 0.91(4) | 1.16(5) |
| $Si_4$ | 0.1812(1) | 0.1814(1) | 0.7129(5) | 0.7132(6) | -0.0143(2) | -0.0151(2) | 0.79(4) | 0.98(4) |
| $Si_5$ | 0.3091(1) | 0.3098(2) | 0.7074(5) | 0.7084(6) | 0.0111(2) | 0.0126(2) | 0.87(4) | 1.15(4) |
| $Si_6$ | 0.3478(1) | 0.3481(2) | 0.2106(5) | 0.2114(5) | -0.0452(2) | -0.0444(2) | 0.77(4) | 1.07(4) |
| $Si_7$ | 0.0416(1) | 0.0420(1) | 0.7963(6) | 0.7942(6) | 0.2188(2) | 0.2193(2) | 0.95(4) | 1.16(4) |
| $Si_8$ | 0.1158(1) | 0.1163(1) | 0.2972(5) | 0.2950(6) | 0.2989(2) | 0.2978(2) | 0.89(4) | 1.13(4) |
| $Si_9$ | 0.2057(1) | 0.2061(1) | 0.3101(6) | 0.3077(6) | 0.2338(2) | 0.2329(2) | 0.92(4) | 1.13(4) |
| $Si_{10}$ | 0.2832(1) | 0.2836(1) | 0.8090(5) | 0.8056(6) | 0.2703(2) | 0.2712(2) | 0.89(4) | 1.12(4) |
| $Si_{11}$ | 0.3676(1) | 0.3687(1) | 0.6995(5) | 0.7012(6) | 0.2003(2) | 0.2016(2) | 0.84(4) | 1.17(4) |
| $Si_{12}$ | 0.4425(1) | 0.4437(1) | 0.1995(5) | 0.2010(6) | 0.2704(2) | 0.2715(2) | 0.88(4) | 1.17(4) |
| $O_1$ | -0.0839(3) | -0.0838(3) | 0.751(1) | 0.752(2) | 0.0131(5) | 0.0116(5) | 1.7(2) | 3.0(2) |
| $O_2$ | -0.0011(3) | -0.0008(3) | 0.896(2) | 0.903(1) | -0.0216(4) | -0.0199(4) | 2.1(2) | 2.6(2) |
| $O_3$ | -0.0129(3) | -0.0122(3) | 0.394(2) | 0.398(1) | 0.0074(4) | 0.0072(5) | 1.7(2) | 2.2(1) |
| $O_4$ | 0.0781(3) | 0.0783(3) | 0.249(2) | 0.249(1) | -0.0109(5) | -0.0105(6) | 2.4(2) | 2.6(2) |
| $O_5$ | 0.1808(2) | 0.1800(3) | 0.413(2) | 0.416(1) | 0.0176(4) | 0.0159(4) | 1.5(1) | 2.0(2) |
| $O_6$ | 0.1663(2) | 0.1657(3) | -0.089(2) | -0.088(1) | 0.0419(4) | 0.0399(4) | 1.3(1) | 1.9(2) |
| $O_7$ | 0.2437(3) | 0.2437(4) | 0.778(1) | 0.774(1) | -0.0081(5) | -0.0074(6) | 1.4(1) | 1.9(1) |
| $O_8$ | 0.3115(2) | 0.3125(3) | 0.410(1) | 0.413(1) | -0.0182(4) | -0.0167(4) | 1.6(1) | 2.1(1) |
| $O_9$ | 0.3287(2) | 0.3289(2) | -0.091(1) | -0.089(1) | -0.0383(3) | -0.0365(4) | 1.1(1) | 1.6(1) |
| $O_{10}$ | 0.0240(3) | 0.0231(3) | 0.745(2) | 0.746(2) | 0.1258(4) | 0.1249(5) | 1.9(1) | 2.3(2) |
| $O_{11}$ | 0.1603(3) | 0.1625(4) | 0.269(2) | 0.267(1) | 0.1380(4) | 0.1378(5) | 1.4(2) | 2.2(2) |
| $O_{12}$ | 0.3518(3) | 0.3527(3) | 0.738(2) | 0.738(1) | 0.1071(4) | 0.1087(5) | 1.9(1) | 2.7(2) |
| $O_{13}$ | -0.0150(3) | -0.0133(3) | 0.750(2) | 0.749(2) | 0.2307(4) | 0.2326(4) | 2.0(1) | 2.6(2) |
| $O_{14}$ | 0.0638(2) | 0.0651(3) | 0.098(2) | 0.095(1) | 0.2417(4) | 0.2423(4) | 1.6(1) | 2.1(1) |
| $O_{15}$ | 0.0934(2) | 0.0939(3) | 0.597(2) | 0.595(1) | 0.2763(4) | 0.2751(4) | 1.7(1) | 2.1(2) |
| $O_{16}$ | 0.1721(3) | 0.1723(3) | 0.251(1) | 0.249(2) | 0.2861(5) | 0.2853(5) | 2.0(2) | 2.5(2) |
| $O_{17}$ | 0.2297(2) | 0.2304(3) | 0.613(1) | 0.607(1) | 0.2507(4) | 0.2502(5) | 1.6(1) | 2.4(2) |
| $O_{18}$ | 0.2595(2) | 0.2595(3) | 0.111(1) | 0.107(1) | 0.2609(4) | 0.2606(4) | 1.5(1) | 2.1(1) |
| $O_{19}$ | 0.3095(3) | 0.3114(3) | 0.757(1) | 0.756(1) | 0.2090(4) | 0.2120(5) | 1.1(2) | 1.8(2) |
| $O_{20}$ | 0.3879(2) | 0.3902(3) | 0.398(2) | 0.403(1) | 0.2279(4) | 0.2299(4) | 1.5(1) | 1.9(2) |
| $O_{21}$ | 0.4190(2) | 0.4197(3) | 0.901(2) | 0.903(1) | 0.2557(4) | 0.2558(4) | 1.9(1) | 2.1(2) |
| $O_{22}$ | 0.1318(3) | 0.1338(3) | 0.242(2) | 0.244(1) | 0.3923(4) | 0.3914(5) | 1.3(2) | 1.9(2) |
| $O_{23}$ | 0.3336(3) | 0.3339(3) | 0.766(2) | 0.763(1) | 0.3613(4) | 0.3629(5) | 2.2(2) | 2.5(2) |
| $O_{24}$ | 0.4755(3) | 0.4769(4) | 0.252(1) | 0.250(2) | 0.3652(4) | 0.3658(5) | 2.5(2) | 3.2(2) |

Si–O distances and Si–O–Si angles are shown as " uncorrected "for those calculated with mean positions of related atoms, and as " corrected "for those corrected for thermal displacement factors of related atoms.

ESDs are shown in parentheses.

[*1] Atoms are all on the general positions of space group *Aa*.

[**2] Fixed through refinements to define the origin.

In the ideal tridymite structure, which may be represented by the mean positions of atoms in HP, $SiO_4$ units join each other by sharing their corner O atoms to form a three–dimensional framework of six–membered rings. For convenience in describing the structure, the three O atoms of a $SiO_4$ unit in a plane of six–membered rings are distinguished from the fourth O, which is off the plane: the former are called the *basal* O atoms and the latter the *apical* O atom. The $SiO_4$ units orient upward and downward alternately in the six–membered rings to form the *tridymite layers*, which are stacked on top of each other by sharing the apical O atoms to form hexagonal chan-

**Table 4.** (Continued.)

(b) Si–O distances (Å)

| Si-O | 25 °C | | 100 °C | | Si-O | 25 °C | | 100 °C | |
|---|---|---|---|---|---|---|---|---|---|
| | Uncorrected | Corrected | Uncorrected | Corrected | | Uncorrected | Corrected | Uncorrected | Corrected |
| $Si_1$-$O_1$ | 1.600(7) | 1.61 | 1.592(9) | 1.61 | $Si_7$-$O_{13}$ | 1.594(8) | 1.60 | 1.580(10) | 1.61 |
| $Si_1$-$O_2$ | 1.589(8) | 1.60 | 1.584(9) | 1.60 | $Si_7$-$O_{14}$ | 1.600(8) | 1.61 | 1.602(8) | 1.60 |
| $Si_1$-$O_3$ | 1.606(8) | 1.61 | 1.610(9) | 1.62 | $Si_7$-$O_{15}$ | 1.608(7) | 1.61 | 1.606(7) | 1.61 |
| $Si_1$-$O_{10}$ | 1.588(8) | 1.60 | 1.572(8) | 1.59 | $Si_7$-$O_{10}$ | 1.584(8) | 1.62 | 1.600(9) | 1.61 |
| Mean | 1.596 | 1.61 | 1.590 | 1.60 | Mean | 1.597 | 1.61 | 1.597 | 1.61 |
| $Si_2$-$O_2$ | 1.605(8) | 1.62 | 1.591(9) | 1.61 | $Si_8$-$O_{14}$ | 1.611(7) | 1.62 | 1.598(8) | 1.61 |
| $Si_2$-$O_3$ | 1.605(8) | 1.61 | 1.591(9) | 1.60 | $Si_8$-$O_{15}$ | 1.594(8) | 1.60 | 1.595(8) | 1.60 |
| $Si_2$-$O_4$ | 1.586(8) | 1.60 | 1.584(9) | 1.60 | $Si_8$-$O_{16}$ | 1.597(8) | 1.61 | 1.590(9) | 1.61 |
| $Si_2$-$O_{24}$ | 1.588(8) | 1.61 | 1.594(9) | 1.62 | $Si_8$-$O_{22}$ | 1.604(8) | 1.61 | 1.595(9) | 1.61 |
| Mean | 1.596 | 1.61 | 1.590 | 1.61 | Mean | 1.602 | 1.61 | 1.595 | 1.61 |
| $Si_3$-$O_4$ | 1.604(8) | 1.62 | 1.599(9) | 1.61 | $Si_9$-$O_{16}$ | 1.601(8) | 1.63 | 1.610(10) | 1.62 |
| $Si_3$-$O_5$ | 1.590(7) | 1.60 | 1.592(8) | 1.60 | $Si_9$-$O_{17}$ | 1.609(7) | 1.61 | 1.597(9) | 1.63 |
| $Si_3$-$O_6$ | 1.599(8) | 1.60 | 1.600(9) | 1.61 | $Si_9$-$O_{18}$ | 1.590(7) | 1.61 | 1.588(8) | 1.61 |
| $Si_3$-$O_{11}$ | 1.581(8) | 1.59 | 1.580(10) | 1.59 | $Si_9$-$O_{11}$ | 1.622(8) | 1.60 | 1.605(9) | 1.60 |
| Mean | 1.594 | 1.60 | 1.593 | 1.60 | Mean | 1.606 | 1.61 | 1.600 | 1.61 |
| $Si_4$-$O_5$ | 1.612(7) | 1.62 | 1.600(8) | 1.61 | $Si_{10}$-$O_{17}$ | 1.594(7) | 1.60 | 1.594(8) | 1.60 |
| $Si_4$-$O_6$ | 1.607(7) | 1.61 | 1.606(8) | 1.62 | $Si_{10}$-$O_{18}$ | 1.609(7) | 1.61 | 1.609(8) | 1.62 |
| $Si_4$-$O_7$ | 1.600(9) | 1.61 | 1.580(10) | 1.59 | $Si_{10}$-$O_{19}$ | 1.592(8) | 1.60 | 1,587(9) | 1.60 |
| $Si_4$-$O_{22}$ | 1.608(7) | 1.61 | 1.601(9) | 1.61 | $Si_{10}$-$O_{23}$ | 1.593(8) | 1.61 | 1.605(9) | 1.62 |
| Mean | 1.607 | 1.61 | 1.597 | 1.61 | Mean | 1.597 | 1.60 | 1.599 | 1.61 |
| $Si_5$-$O_7$ | 1.597(9) | 1.60 | 1.610(10) | 1.62 | $Si_{11}$-$O_{19}$ | 1.611(7) | 1.60 | 1.608(9) | 1.60 |
| $Si_5$-$O_8$ | 1.592(7) | 1.60 | 1.586(8) | 1.60 | $Si_{11}$-$O_{20}$ | 1.599(8) | 1.61 | 1.594(8) | 1.62 |
| $Si_5$-$O_9$ | 1.594(7) | 1.60 | 1.587(7) | 1.59 | $Si_{11}$-$O_{21}$ | 1.600(7) | 1.60 | 1.595(7) | 1.60 |
| $Si_5$-$O_{12}$ | 1.604(8) | 1.62 | 1.609(9) | 1.63 | $Si_{11}$-$O_{12}$ | 1.588(8) | 1.61 | 1.580(10) | 1.60 |
| Mean | 1.597 | 1.60 | 1.598 | 1.61 | Mean | 1.600 | 1.61 | 1.594 | 1.60 |
| $Si_6$-$O_1$ | 1.595(7) | 1.60 | 1.589(8) | 1.61 | $Si_{12}$-$O_{13}$ | 1.601(8) | 1.61 | 1.600(10) | 1.62 |
| $Si_6$-$O_8$ | 1.602(7) | 1.61 | 1.604(8) | 1.61 | $Si_{12}$-$O_{20}$ | 1.602(7) | 1.61 | 1.596(7) | 1.60 |
| $Si_6$-$O_9$ | 1.609(7) | 1.61 | 1.613(7) | 1.62 | $Si_{12}$-$O_{21}$ | 1.588(8) | 1.60 | 1.590(8) | 1.60 |
| $Si_6$-$O_{23}$ | 1.618(8) | 1.63 | 1.600(10) | 1.62 | $Si_{12}$-$O_{24}$ | 1.576(8) | 1.60 | 1.568(9) | 1.59 |
| Mean | 1.606 | 1.61 | 1.602 | 1.61 | Mean | 1.592 | 1.60 | 1.589 | 1.60 |

Mean Si–O (uncorrected) *: 1.599Å at 25 ℃ and 1.595 Å at 100 ℃.
Mean Si–O (corrected) *: 1.61 Å at 25 and 100 ℃.
Uncorrected values are shown with ESDs in parentheses.
ESDs for corrected ones are all 0.02 Å.
* Unbiased sample means.

nels along the *c*–axis. Looking down the tridymite layer of MC or OP along the pseudohexagonal *c*–axis, the six–membered rings are seen to be distorted into a ditrigonal shape and an oval one, denoted as D (or D ′in another orientation) and O (or O ′), respectively. These distortions cause the Si–O–Si bonds to bend so as to be divided into two groups: one, denoted as Si–O–Si(∥), with the basal O atom is more bent, nearly in (001), and the other, Si–O–Si(⊥), with the apical O atom is less bent, nearly along the normal to the tridymite layers. Figure 7 shows the two–series of the temperature dependences of the equivalent isotropic temperature factors $B_{eq}$ for O atoms, each averaged over all the O atoms (solid circles) and the apical O atoms (open triangles), together with those for the Si atoms (crosses).

The atomic coordinates obtained from the harmonic refinements of X–ray diffraction intensities may represent the mean positions of atoms. The calculated distances for such positions, i.e., the inter–mean distances, may possibly differ more or less from those of real bonds.

**Table 4.** (Continued.)

(c) Si–O–Si angles (°)

| Si-O-Si | 25 °C | | 100 °C | |
|---|---|---|---|---|
| | Uncorrected | Corrected | Uncorrected | Corrected |
| $Si_1$-$O_1$-$Si_6$ | 153.9(6) | 151(2) | 156.4(8) | 150(2) |
| $Si_1$-$O_2$-$Si_2$ | 147.6(5) | 145(1) | 149.6(6) | 146(1) |
| $Si_2$-$O_3$-$Si_1$ | 145.9(5) | 144(1) | 147.1(6) | 144(1) |
| $Si_2$-$O_4$-$Si_3$ | 155.1(6) | 151(2) | 155.9(7) | 152(2) |
| $Si_3$-$O_5$-$Si_4$ | 144.4(6) | 143(1) | 145,8(6) | 144(1) |
| $Si_3$-$O_6$-$Si_4$ | 142.4(5) | 141(1) | 143.2(6) | 141(1) |
| $Si_4$-$O_7$-$Si_5$ | 154.4(5) | 153(2) | 155.9(6) | 154(2) |
| $Si_5$-$O_8$-$Si_6$ | 143.9(5) | 142(1) | 145.1(5) | 143(1) |
| $Si_5$-$O_9$-$Si_6$ | 146.0(5) | 145(1) | 147.0(5) | 146(1) |
| $Si_1$-$O_{10}$-$Si_7$ | 157.5(5) | 154(2) | 158.9(6) | 154(2) |
| $Si_3$-$O_{11}$-$Si_9$ | 151.3(6) | 150(2) | 154.5(7) | 151(2) |
| $Si_5$-$O_{12}$-$Si_{11}$ | 152.6(5) | 149(1) | 152.9(6) | 149(2) |
| $Si_7$-$O_{13}$-$Si_{12}$ | 155.5(5) | 152(2) | 156.7(6) | 152(2) |
| $Si_7$-$O_{14}$-$Si_8$ | 147.6(5) | 145(1) | 148.9(6) | 146(1) |
| $Si_7$-$O_{15}$-$Si_8$ | 147.6(5) | 147(1) | 148.0(5) | 147(1) |
| $Si_8$-$O_{16}$-$Si_9$ | 148.3(6) | 145(1) | 148.4(6) | 145(2) |
| $Si_9$-$O_{17}$-$Si_{10}$ | 147.0(5) | 147(l) | 148.2(6) | 146(1) |
| $Si_9$-$O_{18}$-$Si_{10}$ | 148.8(5) | 146(1) | 149.6(5) | 148(1) |
| $Si_{10}$-$O_{19}$-$Si_{11}$ | 145.9(5) | 145(1) | 148.4(6) | 147(2) |
| $Si_{11}$-$O_{20}$-$Si_{12}$ | 145.5(5) | 144(1) | 147.6(5) | 146(1) |
| $Si_{11}$-$O_{21}$-$Si_{12}$ | 147.0(5) | 145(1) | 148.0(5) | 146(1) |
| $Si_4$-$O_{22}$-$Si_8$ | 148.5(5) | 147(1) | 151.6(6) | 149(2) |
| $Si_6$-$O_{23}$-$Si_{10}$ | 145.2(5) | 142(1) | 145.6(6) | 142(1) |
| $Si_2$-$O_{24}$-$Si_{12}$ | 178.0(7) | 162(3) | 179.5(8) | 160(3) |
| Mean Si-O-Si(‖)* | 148.2 | 146 | 149.4 | 147 |
| Mean Si-O-Si(⊥)* | 155.5 | 151 | 157.2 | 151 |
| Mean Si-O-Si* | 150.0 | 147 | 151.4 | 148 |

ESDs are in parentheses.

* Unbiased sample means.

In the present study, the inter–mean distances for Si–O, Si–Si and O–O and angles for Si–O–Si were firstly calculated, and then the inter–mean distances for Si–O were corrected using the analysis of Downs et al. (1990), a rigid–body analysis based on the anisotropic mean square displacements (MSD) of each pair of atoms. The Si–O–Si angles were also calculated from the Si–Si inter–mean distances and the corrected Si–O distances. We refer to the distances and angles for mean positions as " uncorrected," and those with corrected values as " corrected."

## OP tridymite

The most remarkable of the OP structure is the highly anisotropic and large MSDs of O atoms. The apical O atoms in the OP structure are numbered from 1 to 3, and the remaining ones, i.e., the basal ones from 4 to 12 (Fig. 6a), following Kihara (1977). For further convenience, the principal axes of thermal ellipsoids are numbered from 1 for the largest to 3 for the smallest. As indicated in Figures 6 and 7, the MSDs of O atoms in the OP structure are much larger (three or four times) and more strongly anisotropic than in MC. In particular, Figure 7 shows that the differences between the apical and basal O atoms are much larger in OP. The axes–1 of thermal ellipsoids for the apical O atoms, which form the nearly straight Si–Oi – Si bonds, are also especially large but are all nearly parallel with [100] (Fig. 7).

The Si–O bond distances show a little variety within each tetrahedron. The means of uncorrected and corrected Si–O distances in the six independent tetrahedra are 1.576 and 1.61Å for the 24 values, respectively. The Si–O–Si angles are around the mean of 154.4 °for Si–O–Si(‖), and 175.0 ° for Si–O–Si(⊥), both for the uncorrected values. With the corrected Si–O distances, these values reduce to 146 ° and 149 °, respectively.

**Table 4.** (Continued.)

(d) O–O distances (Å) in $SiO_4$

| Central Si | O-O pair | 25 °C | | | 100 °C | | |
|---|---|---|---|---|---|---|---|
| $Si_1$ | $O_1$-$O_2$, $O_1$-$O_3$, $O_1$-$O_{10}$, | 2.61, | 2.60, | 2.59, | 2.59, | 2.59, | 2.58, |
| | $O_2$-$O_3$, $O_2$-$O_{10}$, $O_3$-$O_{10}$ | 2.61, | 2.60, | 2.62 | 2.62, | 2.58, | 2.60 |
| $Si_2$ | $O_2$-$O_3$, $O_2$-$O_4$, $O_2$-$O_{24}$, | 2.60, | 2.64, | 2.58, | 2.57, | 2.63, | 2.59 |
| | $O_3$-$O_4$, $O_3$-$O_{24}$, $O_4$-$O_{24}$ | 2.63, | 2.61, | 2.58 | 2.62, | 2.61, | 2.56 |
| $Si_3$ | $O_4$-$O_5$, $O_4$-$O_6$, $O_4$-$O_{11}$, | 2.59, | 2.63, | 2.58, | 2.59, | 2.62, | 2.60, |
| | $O_5$-$O_6$, $O_5$-$O_{11}$, $O_6$-$O_{11}$ | 2.61, | 2.62, | 2.58 | 2.62, | 2.61, | 2.57 |
| $Si_4$ | $O_5$-$O_6$, $O_5$-$O_7$, $O_5$-$O_{22}$, | 2.59, | 2.63, | 2.64, | 2.58, | 2.61, | 2.63, |
| | $O_6$-$O_7$, $O_6$-$O_{22}$, $O_7$-$O_{22}$ | 2.65, | 2.62, | 2.62 | 2.64, | 2.62, | 2.59 |
| $Si_5$ | $O_7$-$O_8$, $O_7$-$O_9$, $O_7$-$O_{12}$, | 2.60, | 2.59, | 2.62, | 2.60, | 2.60, | 2.64, |
| | $O_8$-$O_9$, $O_8$-$O_{12}$, $O_9$-$O_{12}$ | 2.60, | 2.63, | 2.62 | 2.61, | 2.62, | 2.61 |
| $Si_6$ | $O_1$-$O_8$, $O_1$-$O_9$, $O_1$-$O_{23}$, | 2.62, | 2.63, | 2.62, | 2.62, | 2.63, | 2.59, |
| | $O_8$-$O_9$, $O_8$-$O_{23}$, $O_9$-$O_{23}$ | 2.59, | 2.65, | 2.62 | 2.58, | 2.65, | 2.61 |
| $Si_7$ | $O_{10}$-$O_{13}$, $O_{10}$-$O_{14}$, $O_{10}$-$O_{15}$, | 2.57, | 2.59, | 2.62, | 2.57, | 2.60, | 2.63, |
| | $O_{13}$-$O_{14}$, $O_{13}$-$O_{15}$, $O_{14}$-$O_{15}$ | 2.62, | 2.63, | 2.61 | 2.61, | 2.62, | 2.60 |
| $Si_8$ | $O_{14}$-$O_{15}$, $O_{14}$-$O_{16}$, $O_{14}$-$O_{22}$, | 2.60, | 2.64, | 2.61, | 2.60, | 2.62, | 2.61, |
| | $O_{15}$-$O_{16}$, $O_{15}$-$O_{22}$, $O_{16}$-$O_{22}$ | 2.62, | 2.60, | 2.62 | 2.61, | 2.59, | 2.59 |
| $Si_9$ | $O_{11}$-$O_{16}$, $O_{11}$-$O_{17}$, $O_{11}$-$O_{18}$, | 2.62, | 2.65, | 2.64, | 2.63, | 2.63, | 2.61, |
| | $O_{16}$-$O_{17}$, $O_{16}$-$O_{18}$, $O_{17}$-$O_{18}$ | 2.61, | 2.61, | 2.60 | 2.61, | 2.60, | 2.59 |
| $Si_{10}$ | $O_{17}$-$O_{18}$, $O_{17}$-$O_{19}$, $O_{17}$-$O_{23}$, | 2.59, | 2.62, | 2.62, | 2.60, | 2.61, | 2.64, |
| | $O_{18}$,$O_{19}$, $O_{18}$-$O_{23}$, $O_{19}$-$O_{23}$ | 2.62, | 2.61, | 2.59 | 2.62, | 2.62, | 2.58 |
| $Si_{11}$ | $O_{12}$-$O_{19}$, $O_{12}$-$O_{20}$, $O_{12}$-$O_{21}$, | 2.59, | 2.61, | 2.61, | 2.59, | 2.60, | 2.59, |
| | $O_{19}$-$O_{20}$, $O_{19}$-$O_{21}$, $O_{20}$-$O_{21}$ | 2.61, | 2.65, | 2.61 | 2.60, | 2.64, | 2.59 |
| $Si_{12}$ | $O_{13}$-$O_{20}$, $O_{13}$-$O_{21}$, $O_{13}$-$O_{24}$, | 2.60, | 2.63, | 2.61, | 2.59, | 2.63, | 2.60, |
| | $O_{20}$-$O_{21}$, $O_{20}$-$O_{24}$, $O_{21}$-$O_{24}$ | 2.59, | 2.60, | 2.56 | 2.60, | 2.59, | 2.56 |
| | Mean* | 2.61 | | | 2.60 | | |

Value for an O–O pair should be read from the corresponding place in the right hand column headed by 25 or 100 ℃.

ESDs are all 0.01 Å.

* Unbiased sample means.

The unit–cell of this structure can be expressed as a sequence of six slabs perpendicular to [100], which are marked with the letter S numbered from 1 to 6 as subscripts in Figure 6a. Three slabs $S_3$, $S_4$ and $S_5$ are connected by sharing $O_4$ and $O_5$, and the same also occurs for the remaining three $S_6$, $S_1$ and $S_2$, by symmetry. We notice that the stacking of the three slabs, each connected by $O_4$ and $O_5$, results in the formation of hexagonal rings in the D (or D′) type distortion. In the OP structure as illustrated in Figure 6a, the sequences DD and D D′ occur in the stacking of $S_6$–$S_1$–$S_2$ and $S_3$–$S_4$–$S_5$, respectively, and these two sequences meet at the $O_6$ sites, resulting in the formation of the O (or O′) type rings in their interfaces. In other words, the O or O′ type rings occur only at the interfaces between the major parts of the D and D′ rings. In this regard, the sites of $O_6$ are unique in comparison with $O_4$, $O_5$, and other O atoms. Its uniqueness is also seen in the Si–$O_6$–Si angle in comparison with the other angles.

**MC tridymite**

The atomic coordinates at 25 ℃ agree with those of Kato and Nukui (1976) within one ESD. The corrections for the bond distances and angles for the atomic MSDs are much smaller than in OP. The corrected Si–O distances and Si–O–Si angles show no notable change with temperature, whereas the uncorrected values show weak

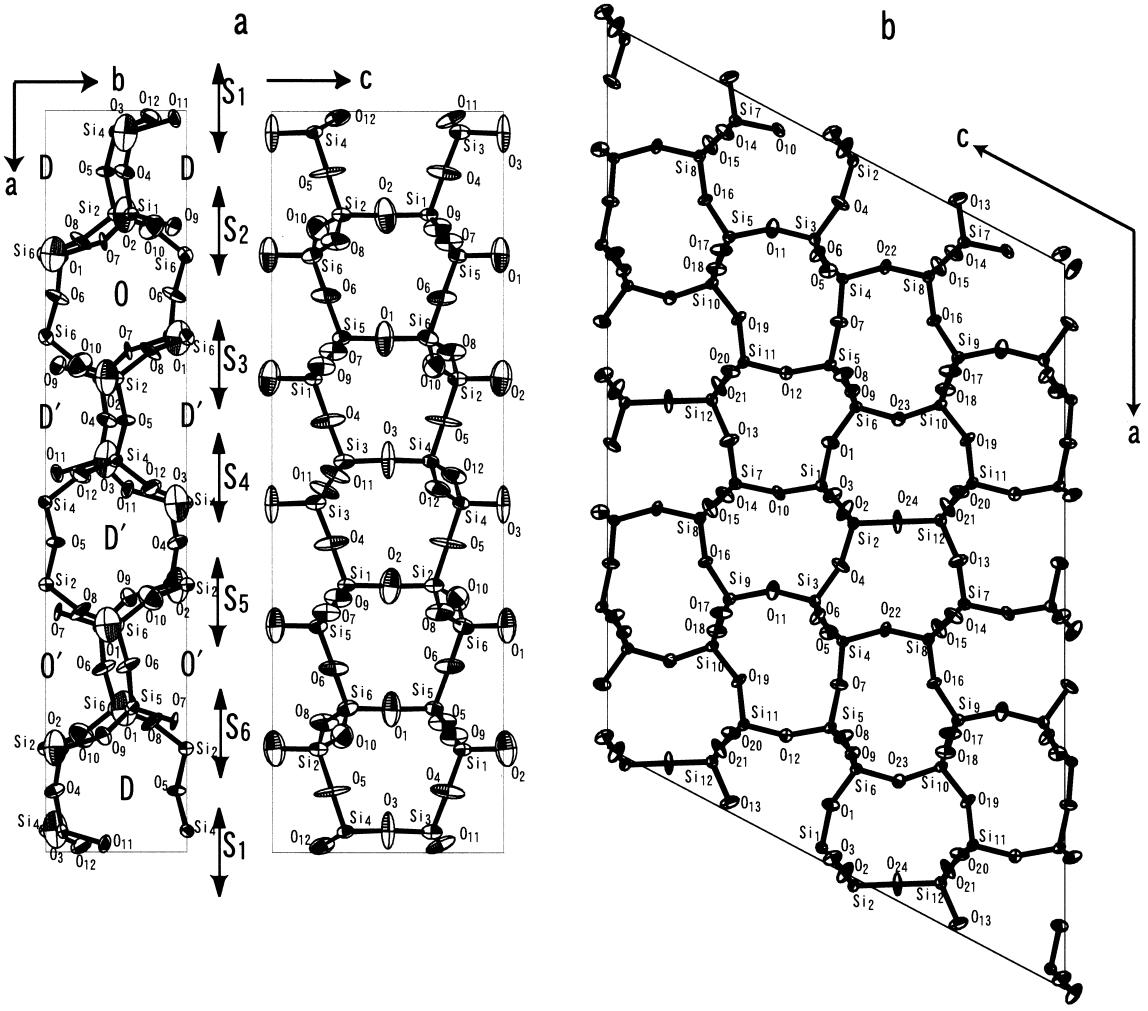


**Figure 6.** Projections of OP and MC structures: **a** OP at 140 ℃ on (001) and (010), and **b** MC at 100 ℃ on (010). Atoms are represented with thermal ellipsoids of 50% probabilities. Ditrigonal– and oval–shaped six–membered rings are marked D or D ′ (in another orientation) and O or O ′ in the (001) projection of OP, which is also associated by symbols from $S_1$ to $S_6$ representing slabs perpendicular to [100].

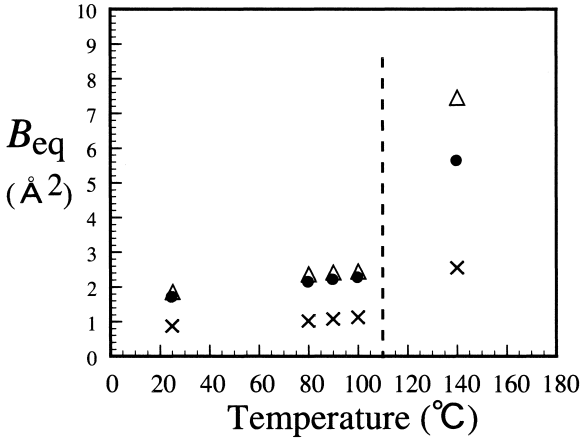


**Figure 7.** Temperature dependence of $B_{eq}$ for O atoms in MC and OP fields. ● : averages over all O atoms, and △ : averages over apical O atoms only. Averages of $B_{eq}$ for Si atoms are indicated with crosses, ×, for comparison. A vertical broken line shows the expected point of the first–order transition between monoclinic and orthorhombic phases.

decreasing and increasing trends, respectively, with increasing temperatures. The mean corrected Si–O distance is 1.61 Å at 25 and 100 ℃, and the corrected values for Si–O–Si angles are 146 (25 ℃) and 147 °(100 ℃) for Si–O–Si(||), and 151 °(25 and 100 ℃) for Si–O–Si(⊥).

Similarly to the unit–cell parameters, the atomic coordinates in MC also change only slightly with temperatures (Table 4). The points for $B_{eq}$ at the four temperatures are well fitted with straight lines for both O and Si atoms, and extrapolations show large gaps to the corresponding points for OP, as illustrated in Figure 7.

In MC, the six–membered rings are distorted similarly as in OP, and each tridymite layer is possibly expressed as the repeat of DDOD D O ′ along its monoclinic [100], just as seen in OP. However, the deformation types are no longer the same just above or below along the pseudohexagonal *c*–axis (or [1/3,0,1]) and, therefore, a similar description to that given for OP is not

applicable to the MC structure.

## DISCUSSION

The present DTA measurements for MC tridymite (TP–a) (Fig. 3) show only the two endothermic peaks at 117 and 166 ℃ (read at the peak tops). The peak at 117 ℃ starts to fall at about 110 ℃ (Fig. 3a), and well corresponds to the significant discontinuities observed between 110 and 115 ℃ in the temperature dependences of unit–cell parameters and Raman scattering profiles. It may be safely concluded that the MC–OP transition takes place over an interval, smaller than 5 ℃, between 110 and 115 ℃. An intermediate phase, if any, has to be found in such a small interval as 5 ℃.

The atomic MSDs in MC are not such as to suggest a clear disorder of atoms: the equivalent isotropic MSDs, $B_{eq}$, averaged over all O atoms, 0.0215 Å$^2$, are larger than 0.0125 Å$^2$ (Kihara, 1990) in quartz at room temperature, but comparable with 0.0181 Å$^2$ (Peacor, 1973) or 0.0235 Å$^2$ (Pluth and Smith, 1985) of low cristobalite at room temperature. The possibility of disorder at the $O_{24}$ site, suggested by Xiao et al. (1993), is not as high as explicitly referred to: the Si–$O_{24}$–Si angle is exceptionally large at 178 (7) ° at 25 ℃, whereas the MSD of $O_{24}$, about 0.031 Å$^2$, is not exceptionally large although it is the largest. The temperature dependences of structural parameters observed in MC tridymite are well fitted with straight lines and, therefore, remarkably different from those observed in low quartz, where the structural parameters involving atomic coordinates and MSDs, cell constants, and so on change rapidly and nonlinearly toward those at the $\alpha$–$\beta$ transition with increasing temperature, being driven by increasing disorder over corresponding Dauphine twin–related sites (Kihara, 2001). The temperature dependences of structural parameters observed in MC, which are rather similar to those in low cristobalite, suggest that the MC structure remains ordered up to the MC–OP transition point, unlike in $\alpha$–quartz.

On the other hand, the characteristic features, in OP, observed in the magnitudes of thermal ellipsoids for $O_4$, $O_5$, $O_6$ and the orientations of their principal axes–1, as well as those of the apical O atoms, may suggest that the rigid $SiO_4$ units undergo librational motions around the axes nearly parallel with [010] passing through the central Si atoms. However, the atomic MSDs increase substantially and abruptly on the OP side of the transition, compared with those in MC. Such large and highly anisotropic MSDs could be accounted for more reasonably by assuming an orientation–disorder of the $SiO_4$ units, as in Kihara (1995), over multiple energy minima, which may be arranged around the directions of principal axes–1 of the thermal ellipsoids of these O atoms. A report about the disorder is in preparation to appear in this journal.

The effects of the anisotropic MSDs of atoms appear in the Si–O distances calculated for the coordinates obtained in the present refinements, which decrease with increasing temperatures. The effects appear more significantly in OP than in MC: the averaged Si–O distances are 1.599 Å at 25 ℃, 1.595 Å at 100 ℃ for MC, but largely reduce to 1.576 Å at 140 ℃ for OP. All these values corrected for the atomic MSDs are about 1.61 Å, in good agreement with the Si–O distances in well–established silica structures.

As indicated with the X–ray diffraction, DTA and Raman measurements, the structure of the monoclinic phase is easily changed to other phases by hand grinding. The present result suggests that measurements with powdered samples may not necessarily be of the MC phase.

## ACKNOWLEDGMENTS

We express sincere thanks to Dr. K. Sakai of Asahi Glass Co., who gave us good quality tridymite samples. This study was supported by the Grant–in–Aid for Scientific Research (C) of JSPS (#14540446).

## REFERENCES

Cellai, D., Carpenter, M.A., Wruck, B. and Salje, E.K.H. (1994) Characterization of high–temperature phase transitions in single crystals of Steinbach tridymite. American Mineralogist, 79, 606–614.

Cellai,D., Carpenter,M.A., Kirkpatrick,R.J., Salie,E.K.H. and Zhang, M. (1995) Thermally Induced Phase Transitions in Tridymite: an Infrared Spectroscopy Study. Physics and Chemistry of Minerals, 22, 50–60.

De Dombal,R.F. and Carpenter, M.A. (1993) High–temperature phase transitions in Steinbach tridymite. European Journal of Mineralogy, 5, 607–622.

Dollase, W. A. (1967) The crystal structure at 220 ℃ of orthorhombic high tridymite from the Steinbach meteorite. Acta Crystallographica, 23, 617–623.

Dollase,W.A and Baur,W.H.(1976) The superstructure of meteoritic low tridymite solved by comturer simulation. American Mineralogist, 61,971–978.

Dollase, W.A. and Buerger, M.J. (1966) Crystal structure of some meteoritic tridymites. Abstracts with Programs of Geological Society of America Annual Meeting, the Geological Society of America, Boulder, CO, 54–55.

Downs, R.T, Gibbs, G.V. Boisen, M.B. Jr. (1990) A study of the mean–square displacement amplitudes of Si, Al, and O atoms in framework structure: Evidence for rigid bonds, order, twinning, and stacking faults. American Mineralogist, 75, 1253–1267.

Graetsch, H. (1998) Characterization of the high–temperature modifications of incommensurate tridymite L3–$T_o$(MX–1)

from 25 to 250 ℃. American Mineralogist, 83, 872–880.
Graetsch, H. (2001) X–ray powder diffraction study on the modulated high temperature forms of $SiO_2$ tridymite between 110 and 220 ℃. Physics and Chemistry of Minerals, 28, 313–321.
Hoffmann, W. (1967) Gitterkonstanten und Raumgruppe von Tridymit bei 20 ℃. Naturwissenshaften, 54, 114–114.
Hoffmann, W., Kockmeyer, M., Löns, J. and Vach, C. (1983) The transformation of monoclinic low–tridymite MC to a phase with an incommensurate superstructure. Fortshritte der Mineralogie, 61, 96–98.
Ito, T. (1973) On the application of a minimum residual method to the structure determination of superstructures. Zeitshrift für Kristallographie, 136, 399–411.
Kato, K. and Nukui, A. (1976) Die Kristallstructur des monoklinen Tief–Tridymits. Acta Crystallographica, B32, 2486–2491.
Kawai, K., Matsumoto, T., Kihara, K. and Sakurai, K. (1978) The first finding of monoclinic tridymite in terrestrial volcanic rocks. Mineralogical Journal, 9, 231–235.
Kihara, K. (1977) An orthorhombic superstructure of tridymite existing between about 105 and 180 ℃. Zeitshrift für Kristallographie, 146, 185–203.
Kihara, K. (1978) Thermal change in unit–cell dimensions, and a hexagonal structure of tridymite. Zeitshrift fur Kristallographie, 148, 237–253.
Kihara, K. (1990) An X–ray study of the temperature dependendce of the quartz structure. European Journal of Mineralogy, 2, 63–77.
Kihara, K. (1995) Disorder and successive structure transitions in the tridymite forms of $SiO_2$. Physics and Chemistry of Minerals, 22,223–232.
Kihara, K. (2001) Molecular dynamics interpretation of structural changes in quartz. Physics and Chemistry of Minerals, 28, 365–376.
Nukui, A. and Nakazawa, H. (1978) Thermal changes in monoclinic tridymite. American Mineralogist, 63, 1252–1259.
Nukui, A. and Nakazawa, H. (1980) Polymorphism in tridymite. Journal of Mineralogical Society of Japan, 14, Special vol. 2, 364–386.
Peacor, D.R. (1973) High–temperature single–crystal study of the cristobalite inversion. Zeitshrift fur Kristallographie, 138, 274–298.
Pluth, J.J. and Smith, J.V. (1985) Crystal structure of low cristobalite at 10, 293, and 473K: Variation of framework geometry with temperature. Journal of Applied Physics, 57, 1045–1049.
Pryde, A.K.A. and Dove, M.T. (1998) On the sequence of phase transitions in tridymite. Physics and Chemistry of Minerals, 26, 171–179.
Schneider, H. and Flolke, O.W. (1982) Microstructure, chemical composition, and structural state of tridymite. Neues Jahrbuch für Mineralogie. Abhandlungen, 145, 280–290.
TEXSAN™ (1989) Structure solution package. The Rigaku Journal, 6, 43–45.
Xiao, Y. Kirkpatrick, R. J. and Kim, Y. J. (1993) Structural phase transitions of tridymite: A $^{29}Si$ MAS NMR investigation. American Mineralogist, 78, 241–244.

*Manuscript received May 18, 2004*
*Manuscript accepted November 1, 2004*
*Manuscript handled by Takashi Murakami*